

SCIENTIFIC REPORTS

OPEN

The expansion of later Acheulean hominins into the Arabian Peninsula

Eleanor M. L. Scerri^{1,2}, Ceri Shipton^{3,4}, Laine Clark-Balzan⁵, Marine Frouin², Jean-Luc Schwenninger², Huw S. Groucutt^{1,2}, Paul S. Breeze⁶, Ash Parton^{7,8}, James Blinkhorn^{1,9}, Nick A. Drake^{1,6}, Richard Jennings¹⁰, Patrick Cuthbertson², Abdulaziz Al Omari¹¹, Abdullah M. Alsharekh¹² & Michael D. Petraglia¹

The Acheulean is the longest lasting cultural–technological tradition in human evolutionary history. However, considerable gaps remain in understanding the chronology and geographical distribution of Acheulean hominins. We present the first chronometrically dated Acheulean site from the Arabian Peninsula, a vast and poorly known region that forms more than half of Southwest Asia. Results show that Acheulean hominin occupation expanded along hydrological networks into the heart of Arabia from Marine Isotope Stage (MIS) 7 until at least ~190 ka — the youngest documented Acheulean in Southwest Asia. The site of Saffaqah features Acheulean technology, characterized by large flakes, handaxes and cleavers, similar to Acheulean assemblages in Africa. These findings reveal a climatically-mediated later Acheulean expansion into a poorly known region, amplifying the documented diversity of Middle Pleistocene hominin behaviour across the Old World and elaborating the terminal archaic landscape encountered by our species as they dispersed out of Africa.

The Acheulean represents a key stage in hominin evolution, characterized by the production of large cutting tools such as handaxes for over ~1.5 million years^{1–5}. Given the rarity of hominin fossils, mapping the chronological and geographic spread of the Acheulean is critical for reconstructing patterns of hominin expansion and evolution in different regions of the Old World. It is also crucial for defining the terminal Acheulean landscape encountered by hominins using Middle Palaeolithic technology, including *Homo sapiens*. However, considerable gaps remain in our understanding of the spatial and temporal distribution of the Acheulean.

Currently, little is known about the Acheulean in the Arabian Peninsula, a critical region situated at the crossroads between Africa and Eurasia. Covering 3.2 million km², the Arabian Peninsula has long been incorporated into narratives of early Eurasian colonization⁶ and numerous Acheulean sites with shared technological characteristics have been documented^{7–10}. However, data required to refine and develop Acheulean dispersal hypotheses has been limited by the fact that the vast majority of documented sites are deflated surface sites lacking stratigraphy and chronometric age estimates. The only known stratified Acheulean site is Saffaqah, situated in the Dawadmi region of the Nejd plateau (Fig. 1). Saffaqah was first identified and excavated by Norman Whalen and colleagues in the 1980s¹¹. Their 33 m² excavation (Trench 1) resulted in the recovery of 8,395 buried artefacts. However, Whalen and colleagues¹¹ did not discuss the stratigraphy nor artefact distributions within the excavations in any detail. They observed calcrete in Trench 1 from 30 cm downwards, while sterile sediment was reached

¹Department of Archaeology, Max Planck Institute for the Science of Human History, Jena, Germany. ²Research Laboratory for Archaeology and the History of Art, School of Archaeology, University of Oxford, 36 Beaumont Street, Oxford, OX1 2PG, UK. ³Centre of Excellence for Australian Biodiversity and Heritage, Australian National University, Canberra, Australia. ⁴British Institute in Eastern Africa, Nairobi, Kenya. ⁵Department of Geosciences, Freiburg, Germany. ⁶Department of Geography, Kings College London, London, UK. ⁷Human Origins and Palaeoenvironments Research Group, Department of Social Sciences, Oxford Brookes University, Headington Campus, Gypsy Lane, Oxford, OX3 0BP, UK. ⁸Mansfield College, University of Oxford, Oxford, OX1 3TF, UK. ⁹Department of Geography Royal Holloway, University of London, Egham, Surrey, TW20 0EX, UK. ¹⁰School of Natural Sciences and Psychology, Liverpool John Moores University, James Parsons Building, Byrom Street, Liverpool, L3 3AF, UK. ¹¹Saudi Commission for Tourism and National Heritage, Riyadh, Saudi Arabia. ¹²Department of Archaeology, College of Archaeology and Tourism, King Saud University, Riyadh, Saudi Arabia. Correspondence and requests for materials should be addressed to E.M.L.S. (email: scerri@shh.mpg.de) or M.D.P. (email: petraglia@shh.mpg.de)

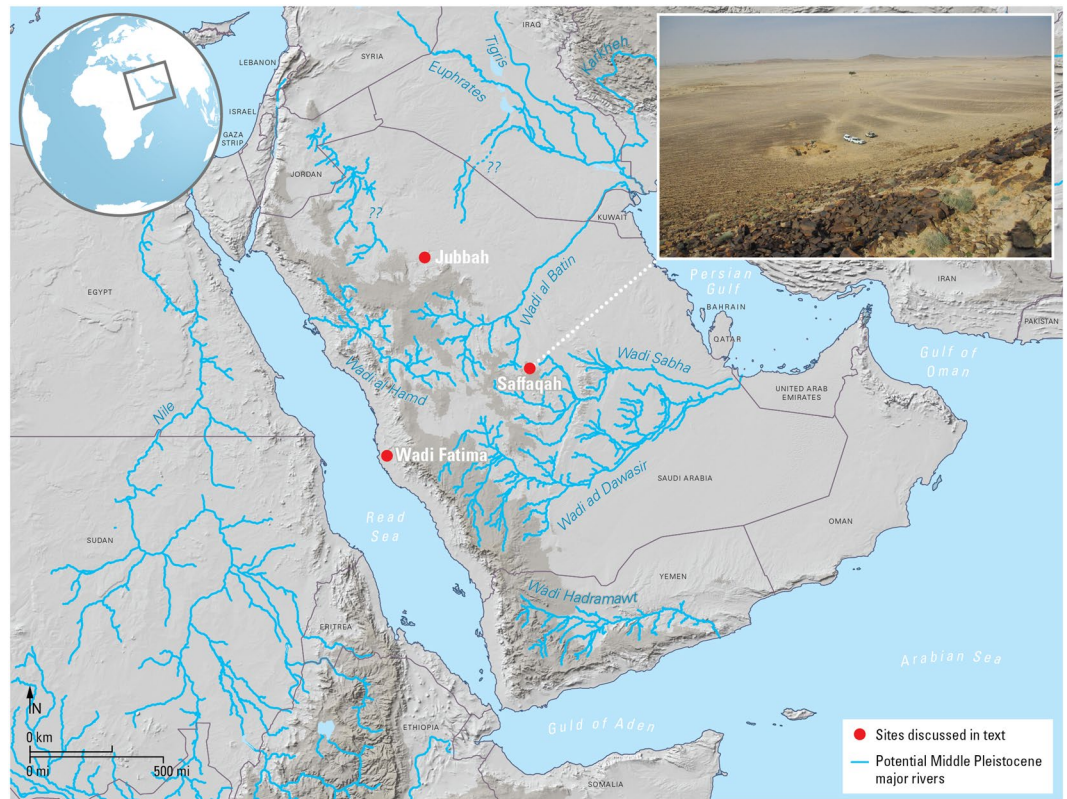


Figure 1. Map showing locations of major river systems and Arabian sites noted in text (a); view of surrounding plain from the top of the andesite dyke: Trench 1 excavations are to the left of the jeeps (b).

at depths of 1.33–1.49 m, and degrading granite bedrock at 1.62 m. Uranium-thorium ages on calcrete adhering to the artefacts suggested that the deposits were at least 200,000 years old, but the ages could not be considered secure (see Methods) and were not further refined.

Given the importance of Saffaqah, a re-assessment of the site's stratigraphy, archaeology and chronology was conducted by the Palaeodeserts Project in 2014 through re-excavation and extension of Trench 1, and a study of the surrounding landscape¹⁰. As reported here, new field investigations now also provide the first secure dates for what is still the only known stratified Acheulean site in the Arabian Peninsula.

Results

The Dawadmi region of central Saudi Arabia is characterized by a flat plain of Proterozoic igneous bedrock intruded by younger felsic and mafic dykes, and overlain in places by Quaternary aeolian and fluvial sediments. The climate is currently arid, although an intensification of the African Summer Monsoon and its incursion into Arabia brought increased summer rainfall to the Peninsula in the past^{12,13}. Palaeoenvironmental records and climate model simulations indicate that increased humidity occurred during insolation maxima, in particular during interglacials and interstadials, such as those during Marine Isotope Stage 7 (MIS 7, ~240–190 ka) and the interstadials of MIS 5 (~130–75 ka)^{12,14}. During these periods, the landscape of Arabia featured extensive river networks, lakes and wetlands with widespread vegetative increases. The Saffaqah site itself is situated near the Central Saudi Arabian town of Dawadmi. It is located beside the most prominent andesite dyke in the region, which rises ~60 m above the surrounding plain and is located on the northern flank of the dyke, below its highest point (Fig. 1). Our systematic survey revealed that Saffaqah is the largest Acheulean site yet documented in Arabia and is surrounded by a dense Acheulean landscape^{10,15}.

Palaeohydrological reconstruction demonstrated that the site sits at the interface between two major extinct river systems: the Wadi al Batin and the Wadi Sabha, major riparian corridors that flowed into the northern and southern ends of the Gulf, respectively (Fig. 1)^{15,16}.

We excavated several test trenches running north downslope from Whalen and colleagues' Trench 1 that confirmed increasingly attenuated stratigraphic sequences lacking buried artefacts. Re-excavation of Trench 1 itself revealed a shallow depression holding *in situ* material, which has infilled to give a thicker stratigraphic sequence and limited post-depositional artefact movement. This depression and its infilling is also clearly visible in piece-plots of the artefacts from Whalen's excavation (Fig. 2). We therefore extended this central part of Trench 1 by 2.5 × 1.5 m (Fig. 3).

Our excavation revealed 1.53 m of sediments within which we identified seven stratigraphic units (A to G, Fig. 3). Both Layer G and the overlying Layer F are archaeologically sterile. A high density accumulation of artefacts in fresh condition, including relatively small pieces, are found concentrated within Layer E, the earliest

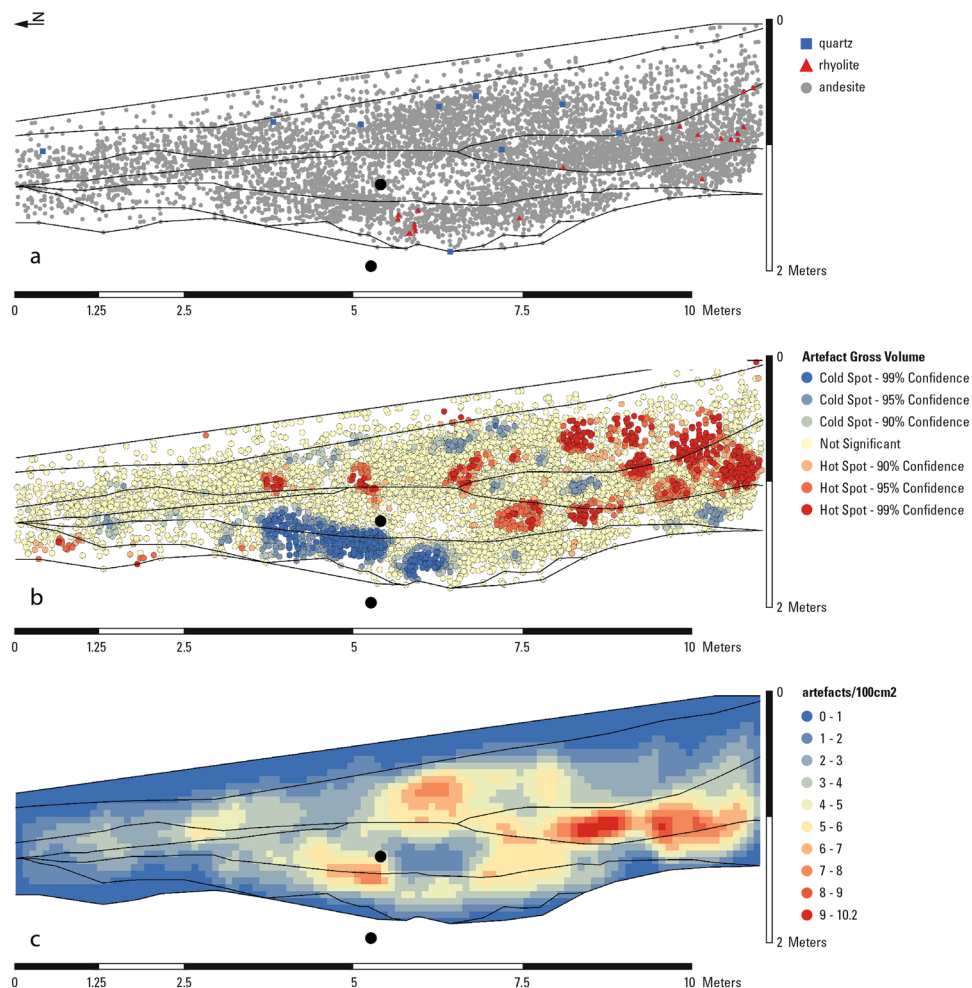


Figure 2. Analysis of the artefact distributions within Trench 1 combining Whalen's¹¹ 3D artefact co-ordinates with the newly recorded stratigraphy showing (a) distribution of artefacts split by raw material types. (b) Hot-Spot analysis of gross artefact volume (L × W × T) indicating concentrations of significantly high and low artefact volumes; (c) total artefact densities. Filled black circles represent the locations of sediment samples for luminescence dating. Modified from Shipton and colleagues¹¹.

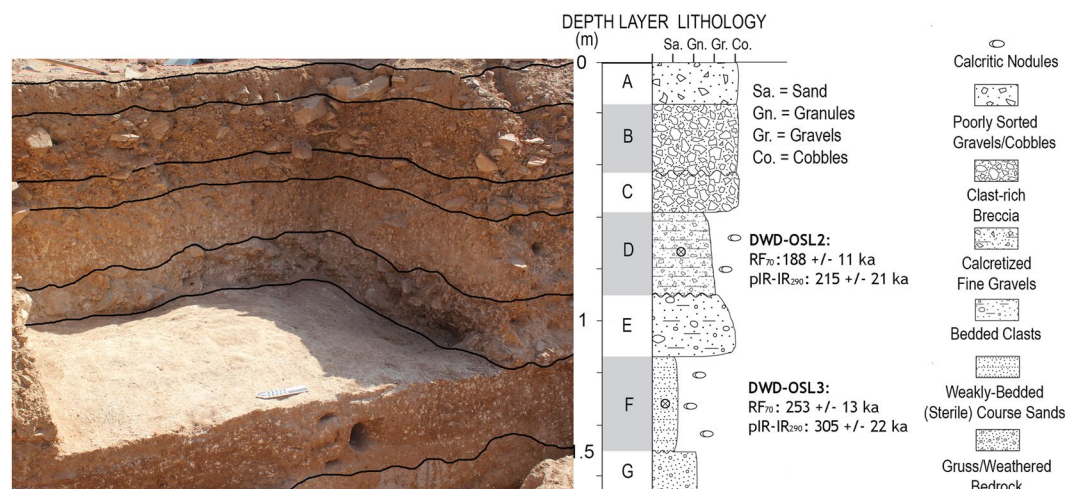


Figure 3. Stratigraphy of Saffaqah, determined from new excavations with sediment samples for luminescence dating bracketing Layer E. Modified from Shipton and colleagues¹¹.

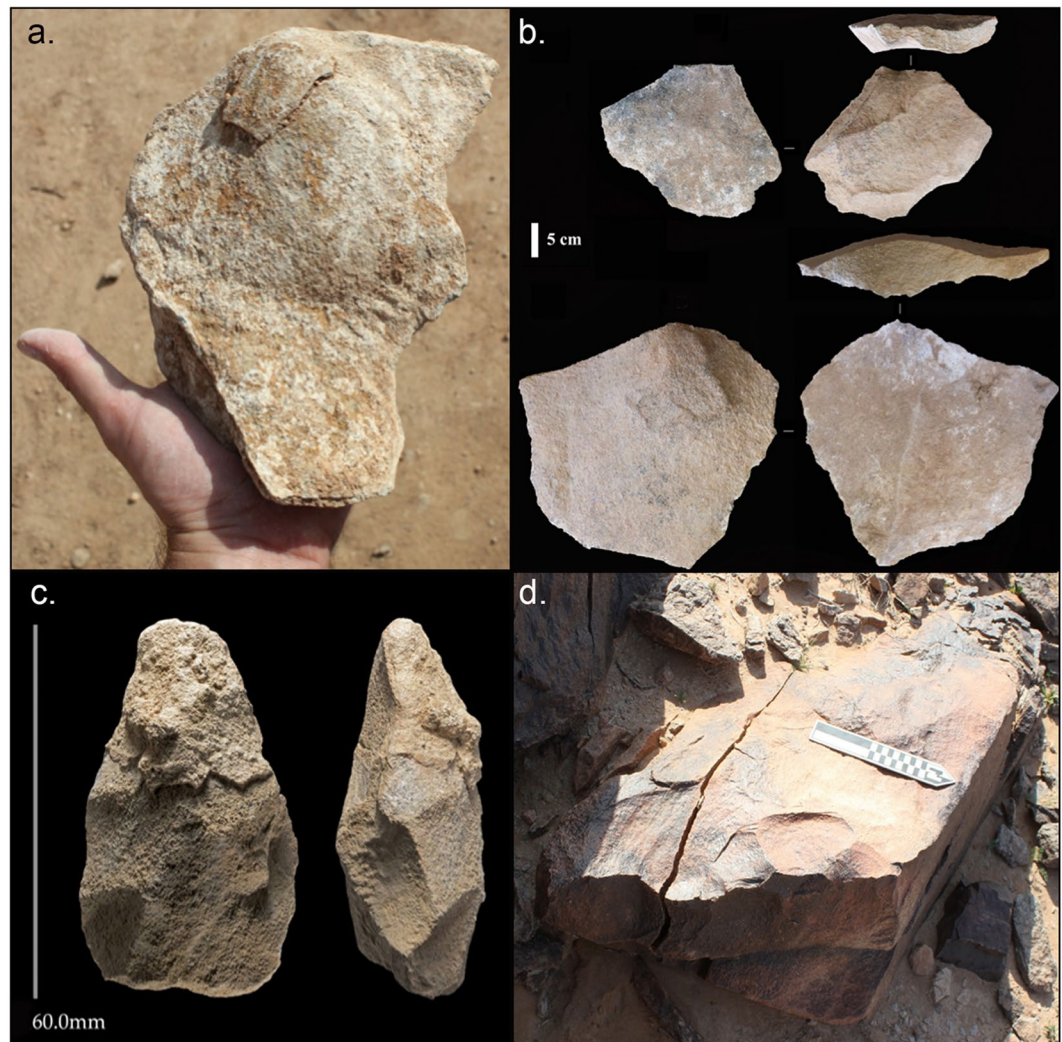


Figure 4. Composite figure of lithics from Saffaqah Layer E, (a) large flake with errillure flake still attached; (b) large flakes; (c) typical handaxe; (d) giant andesite core. Modified from Shipton and colleagues¹¹.

hominin occupation of the site, matching comparable evidence from Whalen's excavation (Figs 2 and 3). Layer E predominately comprises andesite artefacts but also included the rare exploitation of rhyolite (Fig. 2). One of the large flakes from Layer E, which was resting on the core from which it had been struck, still had its errillure flake adhering to it (Fig. 4a) indicating that the artefacts appear to be in effectively the same positions in which they were discarded by hominins.

This initial occupation was buried by finer sediment with lower artefact densities (Layer D). The overlying deposit (Layer C) is the first of three colluvial horizons that includes a distinct concentration of both large and small artefacts, as well as a second concentration of rhyolite artefacts. Lower artefact densities are observed in Layer B, which contains discrete clusters of larger artefacts and dispersed evidence for quartz exploitation.

Sediment samples were collected for luminescence dating within Layers F and D of the freshly excavated trench, two layers bracketing the basal high-density *in situ* lithics in Layer E (Figs 2, 3 and 5, Tables 1–3). Samples were analysed using the post-IR elevated temperature (290 °C) infrared protocol (pIRIR₂₉₀)^{17–19} and the infrared-radiofluorescence protocol at controlled temperature (RF₇₀)^{20,21} (See Methods). pIRIR₂₉₀ and RF₇₀ De dispersions are shown in Fig. 5 and corresponding age estimates are consistent at 2 sigma, providing an average age of ~276 ka for the sterile Layer F and ~197 ka for Layer D.

These dates, together with the fact that central Arabia was predominantly arid during global glacial periods, indicate that artefact deposition in the intermediary Layer E occurred at the beginning of the MIS 7 interglacial. During this time, riparian and lacustrine networks of the Arabian interior were activated following an eastward extension of the African Summer Monsoon system^{15,22,23}. The sharp contact between Layers F and E, and a very diffuse contact between Layers E and D also supports the notion of a quasi-continuous phase of deposition between E and D during MIS 7 and into the beginning of MIS 6.

Our new excavations at Saffaqah resulted in the recovery of over 500 lithic artefacts in stratified context. These are described in detail in Shipton and colleagues¹⁰. This assemblage is dominated by large flakes (the largest

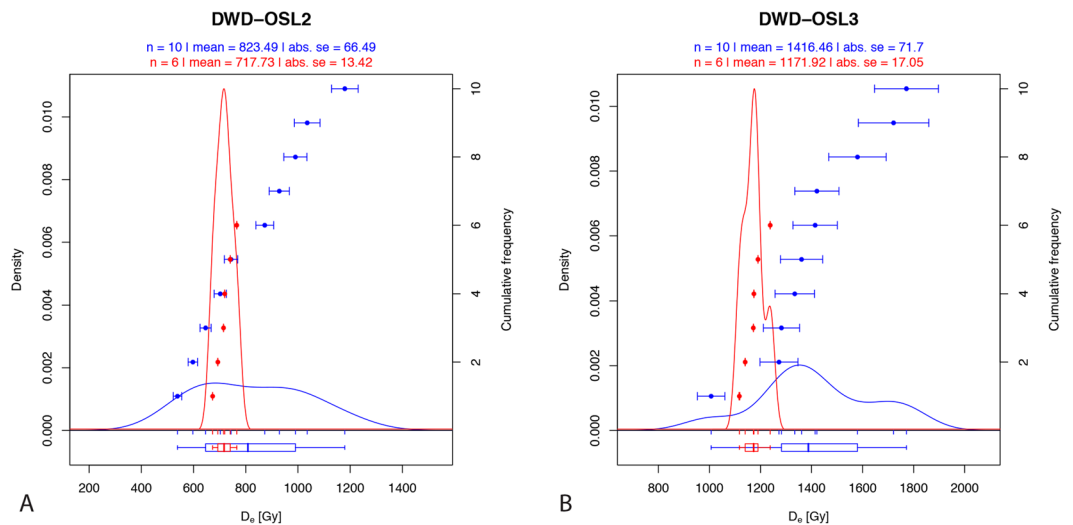


Figure 5. Kernel density estimate of the pIRIR₂₉₀ (blue) and RF₇₀ (red) equivalent doses (dots) and associated error bars in ascending order. The boxplot shows the distribution parameters (median as bold line, box delimited by the first and third quartile, whiskers defined by the extremes). The plot was obtained from the R (R Development Core Team, 2015) package ‘Luminescence’ version 0.8.2^{60–62}.

Sample	Burial depth (m)	Radioelement content			Dose rate (Gy ka ⁻¹)			
		K (%)	Th (ppm)	U (ppm)	Ext gamma	Ext. beta	Ext. alpha	Total
DWD-OSL2	0.85	2.0	8.0	2.0	1.06 ± 0.05	1.90 ± 0.05	0.07 ± 0.01 <i>0.06 ± 0.01</i>	3.83 ± 0.21 <i>3.82 ± 0.22</i>
DWD-OSL3	1.45	2.2	11.1	3.0	1.57 ± 0.08	2.24 ± 0.06	0.11 ± 0.02 <i>0.09 ± 0.02</i>	4.65 ± 0.24 <i>4.63 ± 0.24</i>

Table 1. Radioelement contents and dose rates from Saffaqah sediment samples. *a*-value is 0.08 ± 0.02 for the pIRIR₂₉₀⁶³ and 0.067 ± 0.012 for RF₇₀⁵⁹. Values in italic are for the RF₇₀ measurements.

Sample	Protocol	#	Recycling Ratio (μ ± 1 σ)	Zero Ratio (μ ± 1 σ)	D _e ± se ^a (Gy)	OD ± se ^b (%)	Age ± se ^c (ka)
DWD-OSL2	pIR-IR ₂₉₀	10	1.01 ± 0.01	1.21 ± 0.18	823.5 ± 66.5	23 ± 6	215 ± 21
	RF ₇₀	6	—	—	717.7 ± 13.4	4 ± 1	188 ± 11
DWD-OSL3	pIR-IR ₂₉₀	10	1.01 ± 0.01	1.16 ± 0.17	1416.5 ± 71.7	9 ± 6	305 ± 22
	RF ₇₀	6	—	—	1171.9 ± 17.1	3 ± 1	253 ± 13

Table 2. SAR characteristic, D_e's measured via the pIRIR₂₉₀ and RF₇₀ protocol and luminescence age estimates. All measured aliquots were accepted for analysis; the rejection criteria applied for the pIRIR₂₉₀ are discussed in the text. ^aUnweighted mean. ^bOverdispersion calculated using the Central Age Model⁵³. ^cCalculated using DRAC v.1.2⁶⁴.

Depth in mm	Age in years USGS	Age in years McMaster
700	204,000 ± 17,000	112,000 ± 15,000
860	189,000 ± 14,000	61,000 ± 9,000
860	189,000 ± 14,000	61,000 ± 9,000

Table 3. Whalen and colleagues¹¹ Uranium-Thorium Ages on ‘caliche rind’ from artefacts from unit U-5. The depth of the samples suggests in unit U-5 suggest the both likely come from the equivalent of our layer D. Dates were measured by B.J. Szabo of the USGS in Denver, and by H.P. Schwarz at McMaster University, Ontario.

measuring 310 by 285 mm) that acted as biface blanks (Fig. 4b). These flakes were detached from large blocks of andesite with considerable force (Fig. 4d). Marginally and ventrally retouched flakes, cleavers and discoidal cores were also present. Biface blanks were also produced through bifacial flaking of appropriate edges on large blocks of andesite. Despite the late Acheulean date, the handaxes are minimally flaked, long (\bar{x} 16 mm, σ 38) and thick (\bar{x} 5 mm, σ 15) (Fig. 4c).

The artefact positioning and stratigraphic observations indicate that the lower, chronologically constrained Layer E represents an occupational surface with *in situ* knapping, while the upper layers represent successive occupations, with some minor colluvial deposition in Layers C-B likely dating to MIS 6. Excavated material exhibited no size sorting, preserving flakes as small as 13 mm, which are not found on the surface. Our spatial plotting of artefacts from Whalen's excavation also showed that materials were unevenly distributed throughout: a small amount of quartz artefacts occurred in the upper layers, and rhyolite artefacts occurred as distinct horizontal clusters in the middle and lower parts of the excavation (Fig. 2).

Discussion

Our results demonstrate an Acheulean presence in the Arabian Peninsula during MIS 7, and illustrate how hominins moved into marginal areas with the onset of environmental amelioration. Saffaqah also documents the youngest yet known Acheulean in Southwest Asia²⁴.

The positioning of Saffaqah at the drainage divide between both the Wadi al Batin and the Wadi Sabha palaeo-drainage systems, suggests that Acheulean hominins were using fluvial networks as dispersal corridors into the Peninsula's interior (Fig. 1)^{13,16,23,25,26}. Technological similarities between Saffaqah and other undated Acheulean sites strongly suggest this dispersal may have been widespread in Arabia. For example, minimally flaked handaxes with large flake blanks and cleavers have been documented in both Wadi Fatima, and the Jubbah area (Fig. 1)^{27,28}, in addition to recently reported Acheulean sites in southern Arabia^{29,30}.

The Acheulean technology from Saffaqah can be contrasted to Acheulean surface assemblages found in the southwestern Nefud Desert⁹. Although undated, these assemblages document very different technological characteristics within an Acheulean tradition. The southwestern Nefud assemblages lack cleavers and any large flake component, despite the apparent availability of large blocks of raw material, and feature handaxes that are highly refined, morphologically pointed and shaped from raw material blocks (*façonnage*). This constellation of technological features is similar to the Late Acheulean in the Levant³¹.

In contrast, the large flakes and cleavers of Saffaqah differ from the pene-contemporaneous Acheuleo-Yabrudian technocomplex of the Levant¹⁰ and are instead features more typical of the African Acheulean^{32,33}. Late Acheulean sites such as Mieso (Ethiopia) are of a similar age to Saffaqah as well as manifesting large flakes and cleavers^{34,35}, although it lacks the fine marginal trimming on its bifaces seen at Mieso. It therefore seems possible that Saffaqah reflects a hominin dispersal from the Horn of Africa following the northeastward migration of the African Summer Monsoon during MIS 7^{34,35}. The similarities in the lithic typologies at Saffaqah across all layers spanning MIS 7 and very probably MIS 6 in the case of layers C-B, are also indicative of cultural continuity at least within the general area of the site. Light colluvial activity within Layers C-B plausibly reflects insolation peaks within MIS 6 (i.e. at ~170 and/or 155 ka), providing climate mechanisms to support a sustained hominin presence in the region during generally arid conditions. The results presented here therefore both extend the known spatial and temporal distribution of Acheulean hominins and document variation in behaviour across an expanded range and timeframe. While the age of the Acheulean sites in other parts of Arabia is not yet confirmed, the techno-typological and chronological similarities between the later Acheulean in Africa and Saffaqah indicate that several waves of dispersal may have structured the Acheulean record of Eurasia³⁶.

Finally, because Saffaqah also represents the youngest yet documented Acheulean in southwest Asia, further insights are provided into the persistence of the last Acheulean hominins, the youngest of which have been documented in India in MIS 6³⁷. At Saffaqah, this Acheulean presence was late enough to overlap with an emerging Middle Palaeolithic, both in the Peninsula as well as in surrounding regions, adding to the spatial diversity of Middle Pleistocene hominin behaviour²², and reflecting the complexity and breadth of biogeographical exchange across the Eurasian gateway. The date of $\sim 188 \pm 11$ ka in Layer D provides a *terminus post quem* for the artefacts in the overlying Layers B-C, suggesting that cultural overlap continued into MIS 6. The broader regional evidence, including the presence of *Homo sapiens* in association with early Middle Palaeolithic tool assemblages at Misliya Cave in the Levant during this time³⁸, provides strong indications that Saffaqah formed part of the terminal archaic landscape first encountered by our species as they dispersed out of Africa. Future research should seek to clarify the spatio-temporal character of the final Acheulean and early Middle Palaeolithic/Stone Age, as well as exploring the reasons for this complex transition.

Methods

Sediment samples for luminescence dating were collected from the freshly opened section by inserting opaque metal tubes. Preparation and analyses were carried out at the Luminescence Dating Laboratory of the Research Laboratory for Archaeology and the History of Art, School of Archaeology, at the University of Oxford under filtered laboratory lighting (low intensity LED lighting with peak emission at 594 nm). After the sample tubes were opened, the light-exposed ends were removed for dose rate determination and the interior, light shielded sediment was retained for luminescence dating. Each sediment sample was prepared in a conventional manner in order to extract sand sized (180–255 μm) potassium (K⁺) feldspar mineral grains. This included wet sieving, hydrochloric acid (10%) and then hydrogen peroxide (30%) digestions, followed by heavy liquid density separation using a solution of sodium polytungstate (2.58 g cm⁻³), and a final second sieving.

For the external dose rate contribution, the beta dose rates were calculated from the uranium, thorium and potassium concentrations determined from a homogenized portion (10 g) of sediment by inductively coupled mass spectrometry (ICP-MS) and inductively coupled atomic emission spectroscopy (ICP-AES) outsourced to an accredited specialist laboratory (Actlabs, Canada). Gamma dose rates were measured on site for both samples with an Inspector 1000 gamma-ray spectrometer fitted with a 2.5' NaI probe and calibrated against the Oxford blocks³⁹ using the threshold technique^{40,41}. The cosmic-ray dose rates were estimated from the equations provided by Prescott and Hutton⁴² taking into account the burial depth of the samples, the sediment density and

the location of the site (altitude, latitude). Water content corrections were calculated assuming a burial average of $10 \pm 4\%$, with correction factors from Zimmerman⁴³. Assuming that each grain comprises $12.5 \pm 0.5\%$ potassium and 400 ± 100 ppm rubidium-87^{44,45}, with absorption factors calculated from Brennan⁴⁶ and the rubidium dose rate from Readhead⁴⁷, an internal feldspar dose rate of 0.91 ± 0.15 Gy. ka⁻¹ was included in the dose rate calculations (Table 1).

Equivalent doses (D_e) were measured for ten multigrain K-feldspar aliquots (1 mm diameter) from each sample using the pIRIR₂₉₀ protocol of Thiel *et al.*¹⁹. Measurements were performed on a *Lexsyg Smart* luminescence reader manufactured by Freiberg Instruments⁴⁸ and fitted with a calibrated beta source delivering 0.134 ± 0.003 Gy.s⁻¹. Aliquots were stimulated with infrared LED's emitting at 850 ± 20 nm (200 mW cm⁻²) and the 410 nm IRSL emission signal was detected with a blue detection window (Schott BG39 3 mm and AHF Brightline HC 414/46 Interference 3.5 mm).

Net pIRIR₂₉₀ signals were calculated by subtracting a mean background (last 50 s of stimulation) from the total signal emitted over the first 2 s⁴⁹. Equivalent doses were calculated from each aliquot using the Analyst (v. 4.11) software developed by Duller^{50–52} and meeting the following criteria: i) detectable net natural test signal greater than three sigma above the background signal; ii) test dose error greater than 20% of the calculated test dose; iii) recycling ratios >10%; iv) calculated zero-ratio >5% of L_N/T_N . Based on previous results from samples collected in the Nefud Desert and discussions in Thiel *et al.*¹⁹ and Buylaert *et al.*⁵³, fading rates were considered to be negligible and ages are uncorrected. All twenty measured aliquots had measurable signals and good SAR characteristics; no aliquots were excluded after application of the rejection criteria and none were found to be in saturation. Figure S1 (see supplementary information) shows a typical feldspar pIRIR₂₉₀ signal and corresponding growth curve. Overdispersion values⁵⁴ were low for both samples, with a value of $23 \pm 6\%$ calculated for DWD-OSL2, and $9 \pm 6\%$ for DWD-OSL3 (Table 1). Investigation of a modern, aeolian-deposited sample has also indicated that well-bleached feldspars have negligible residual pIRIR₂₉₀ signal (~1 Gy).

D_e 's were also measured using infrared-radiofluorescence (IR-RF). The IR-RF signal of K-feldspar is believed to provide a promising alternative to more established luminescence dating approaches. The technique was introduced by Trautmann *et al.*⁵⁵ and Erfurt & Krbetschek²⁰ and a reinvestigation of the IR-RF signal characteristics recently led to an improved measurement protocol, which requires keeping the temperature constant at 70 °C during measurement^{21,56,57}.

IR-RF measurements were carried out on a Freiberg Instruments Lexsyg Research reader⁴⁸ equipped with a specially designed ⁹⁰Sr/⁹⁰Y ring-source⁵⁸ delivering 0.057 ± 0.003 Gy.s⁻¹. IR-RF signal detection was made through a Chroma D850/40 interference filter. For bleaching, we used the built-in solar simulator equipped with different LEDs: 365 nm, max. 70 mW cm⁻²; 462 nm, max. 110 mW cm⁻²; 525 nm, max. 45 mW cm⁻²; 590 nm, max. 30 mW cm⁻²; 625 nm, max. 90 mW cm⁻²; 850 nm, max. 170 mW cm⁻². All bleaching and measurement settings followed the suggestions made by Frouin *et al.*²¹ and the D_e values were obtained using the function analyse IRSAR.RF from the R 'Luminescence' package^{21,59}. Figure S2 (see supplementary information) shows the results of the RF₇₀ measurements for the two samples. For both samples, the overdispersion values are less than 5%, indicating that the RF₇₀ signal has been sufficiently bleached. We note that the pIRIR₂₉₀ and RF₇₀ age estimates are consistent at 2 sigma and in stratigraphic order (Table 2).

The only independent age data available for this site consists of uranium-series dating performed upon three samples of 'caliche rind' collected from the underside of lithics excavated by Whalen and colleagues¹¹. These dates are summarized in Table 3. Little information is available concerning the methodology of this study, as it was published as a work in progress. Therefore, the large age difference obtained for subsamples from the same tool is not explicable at the moment, but may be due to varying pre-treatments upon contaminated caliche rinds¹¹. Because of this, and due to the nature of the samples (post-depositional carbonate concretion), these ages must certainly be considered as minimum estimates. While not fully reliable, these calculated ages do not conflict with the current pIRIR₂₉₀ and RF₇₀ age estimates. It is also important to note that, although these values indicate that there is post-depositional enrichment of the uranium component in the sediment, the proportion of the dose rate contributed by the uranium series in this environment is quite low. Therefore, any decay chain disequilibrium is expected to have a negligible effect on the calculated ages. Interestingly Whalen and colleagues¹¹ observed that this 'caliche rind' exclusively occurred on the underside of artefacts, suggesting that however old it is, the artefacts have not moved since deposition.

Data Availability

Luminescence data generated during the current study are available from M.F. and J.-L.S. upon reasonable request.

References

- Schick, K. & Clark, J. D. Biface technological development and variability in the Acheulean Industrial Complex in the Middle Awash region of the Afar Rift, Ethiopia. In *Multiple approaches to the study of bifacial technologies* (eds Soressi, M., Dibble, H. L.) 1–30 (Univ. of Pennsylvania Museum, 2003).
- Dennell, R. *The Palaeolithic Settlement of Asia* (Cambridge University Press, 2009).
- Lepre, C. J. *et al.* An Earlier Origin for the Acheulean. *Nature* **477**, 82–85 (2011).
- Beyene, Y. *et al.* The characteristics and chronology of the earliest Acheulean at Konso, Ethiopia. *PNAS* **110**, 1584–1591 (2012).
- Stout, D., Hecht, E., Khreisheh, N., Bradley, B. & Chaminade, T. Cognitive Demands of Lower Paleolithic Toolmaking. *PLoS One* **10**, e0121804 (2015).
- Bar-Yosef, O. & Belfer-Cohen, A. From Africa to Eurasia – early dispersals. *Quatern. Int* **75**, 19–28 (2001).
- Petraglia, M. D. The Lower Paleolithic of the Arabian Peninsula: occupations, adaptations, and dispersals. *J. World. Prehist.* **17**, 141–179 (2003).
- Groucutt, H. S. & Petraglia, M. D. The Prehistory of the Arabian Peninsula: Deserts, Dispersals, and Demography. *Evo. Anth.* **21**, 113–125 (2012).

9. Scerri, E. M. L. *et al.* Middle to Late Pleistocene human habitation in the western Nefud Desert, Saudi Arabia. *Quatern. Int.* **382**, 200–214 (2015).
10. Shipton, C. *et al.* Acheulean technology and landscape use at Dawadmi, central Arabia. *PLoS ONE* **13**, e0200497 (2018).
11. Whalen, N., Siraj-Ali, J. S. & Davis, W. Excavation of Acheulean sites near Saffaqah, Saudi Arabia, 1403 AH 1983. *Atlat* **8**, 9–24 (1984).
12. Jennings, R. P. *et al.* The greening of Arabia: Multiple opportunities for human occupation of the Arabian Peninsula during the Late Pleistocene inferred from an ensemble of climate model simulations. *Quatern. Int.* **382**, 181–199 (2015).
13. Parton, A. *et al.* Alluvial fan records from southeast Arabia reveal multiple windows for human dispersal. *Geology* **43**, 295–298 (2015).
14. Fleitmann, D. *et al.* Holocene and Pleistocene pluvial periods in Yemen, southern Arabia. *Quatern. Sci. Rev.* **30**, 783–787 (2011).
15. Jennings, R. P. *et al.* Multi-scale Acheulean landscape survey in the Arabian Desert. *Quatern. Int.* **382**, 58–81 (2015).
16. Petraglia, M. D., Drake, N. & Alsharekh, A. Acheulean landscapes and large cutting tool assemblages in the Arabian Peninsula. In *The Evolution of Human Populations in Arabia* (eds Petraglia, M. D., Rose, J. I.) 103–116 (Springer, 2009).
17. Thomsen, K. J., Murray, A. S., Jain, M. & Botter-Jensen, L. Laboratory fading rates of various luminescence signals from feldspar-rich sediment extracts. *Radiat. Meas.* **43**, 1474–1486 (2008).
18. Buylaert, J. P., Murray, A. S., Thomsen, K. J. & Jain, M. Testing the potential of an elevated temperature IRSL signal from K-feldspar. *Radiat. Meas.* **44**, 560–565 (2009).
19. Thiel, C. *et al.* Luminescence dating of the Stratzing loess profile (Austria)—Testing the potential of an elevated temperature post-IR IRSL protocol. *Quatern. Int.* **234**, 23–31 (2011).
20. Erfurt, G. & Krbetschek, M. R. IRSAR—a single-aliquot regenerative-dose dating protocol applied to the infrared radiofluorescence (IR-RF) of coarse-grain K-feldspar. *Ancient TL* **21**, 35 (2003).
21. Frouin, M. *et al.* An improved radiofluorescence single-aliquot regenerative dose protocol for K-feldspars. *Quat. Geochronol.* **38**, 13–24 (2017).
22. Petraglia, M. D. *et al.* Hominin dispersal into the Nefud desert and middle Palaeolithic settlement along the Jubbah palaeolake, northern Arabia. *PLoS One* **7**, e49840 (2012).
23. Rosenberg, T. M. *et al.* Late Pleistocene palaeolake in the interior of Oman: A potential key-area for the dispersal of anatomically modern humans out-of-Africa? *J Quatern Sci* **27**, 13–16 (2012).
24. Sharon, G. The Acheulian of the Levant. In: Enzel, Y., Bar-Yosef, O. (Eds), *Quaternary of the Levant*, pp. 539–547 Cambridge University Press, Cambridge (2017).
25. Breeze, P. S. *et al.* Remote sensing and GIS techniques for reconstructing Arabian palaeohydrology and identifying archaeological sites. *Quatern. Int.* **382**, 98–119 (2015).
26. Breeze, P. S. *et al.* Palaeohydrological corridors for hominin dispersals in the Middle East ~250–70,000 years ago. *Quatern. Sci. Rev.* **144**, 155–185 (2016).
27. Whalen, N., Siraj-Ali, J., Sindi, H. O., Pease, D. W. & Badein, M. A. A complex of sites in the Jeddah-Wadi Fatimah area. *Atlat* **11**, 77–85 (1988).
28. Shipton, C. *et al.* Large flake Acheulean in the Nefud Desert of northern Arabia. *PaleoAnth.* **2014**, 446–462 (2014).
29. Bretzke, K., Yousif, E. & Jasim, S. Filling in the gap – The Acheulean site Suhailah 1 from the central region of the Emirate of Sharjah, UAE. *Quatern. Int.* **466**, 23–32 (2018).
30. Foulds, F. *et al.* A large handaxe from Wadi Dabsa and early hominin adaptations within the Arabian Peninsula. *Antiquity* **91**, 1421–1434 (2017).
31. Gisis, I. & Ronen, A. Bifaces from the Acheulian and Yabrudian layers of Tabun cave, Israel. In *Axe Age, Acheulian Tool-Making from Quarry to Discard* (eds Goren-Inbar, N., Sharon, G.) 137–154 (London: Equinox, 2006).
32. Gamble, C. & Marshall, Y. The shape of handaxes, the structure of the Acheulean World. In *A Very Remote Period Indeed* (eds Milliken, S., Cook, J.) 19–27 (Oxbow Books, 2001).
33. Sahnouni, M., Semaw, S. & Rogers, M. The African Acheulean: An Archaeological Summary. In *The Oxford Handbook of African Archaeology* (eds Mitchell, P., Lane, P.J.) doi:0.1093/oxfordhb/9780199569885.013.0022 (2013).
34. Benito-Calvo, A., Barfod, D. N., McHenry, L. J. & de la Torre, I. The geology and chronology of the Acheulean deposits in the Mieso area (East-Central Ethiopia). *J. Hum. Evol.* **76**, 26–38 (2014).
35. de la Torre, I., Mora, R., Arroyo, A. & Benito-Calvo, A. Acheulean technological behaviour in the middle Pleistocene landscape of Mieso (East-Central Ethiopia). *J. Hum. Evol.* **76**, 1–25 (2014).
36. Goren-Inbar, N. *et al.* Pleistocene milestones on the out-of-Africa corridor at Gesher Benot Ya'akov, Israel. *Science* **289**, 944–947 (2000).
37. Haslam, M. *et al.* Late Acheulean hominins at the Marine Isotope Stage 6/5e transition in north-central India. *Quatern. Res.* **75**, 670–682 (2011).
38. Hershkovitz, I. *et al.* The earliest modern humans outside Africa. *Science* **359**, 456–459 (2018).
39. Rhodes, E. J. & Schwenninger, J.-L. Dose rates and radioisotope concentrations in the concrete calibration blocks at Oxford. *Ancient TL* **25**, 5–8 (2007).
40. Mercier, N. & Falguères, C. Field gamma dose-rate measurement with a NaI (Tl) detector: re-evaluation of the “threshold” technique. *Ancient TL* **25**, 1–4 (2007).
41. Duval, M. & Arnold, L. J. Field gamma dose-rate assessment in natural sedimentary contexts using LaBr 3 (Ce) and NaI (Tl) probes: a comparison between the “threshold” and “windows” techniques. *Appl. Radiat. Isot.* **74**, 36–45 (2013).
42. Prescott, J. R. & Hutton, J. T. Cosmic ray contributions to dose rate for luminescence and ESR dating: Large depths and long-term time variations. *Radiat. Meas.* **23**, 497–500 (1994).
43. Zimmerman, D. W. Thermoluminescence dating using fine grains from pottery. *Archaeometry* **13**, 29–52 (1971).
44. Huntley, D. J. & Baril, M. R. The K content of the K-feldspars being measured in optical dating or in thermoluminescence dating. *Ancient TL* **15**, 11–13 (1997).
45. Huntley, D. J. & Hancock, R. G. V. The Rb contents of the K-feldspar grains being measured in optical dating. *Ancient TL* **19**, 43–46 (2001).
46. Brennan, B. J. Beta doses to spherical grains. *Radiat. Meas.* **37**, 299–303 (2003).
47. Readhead, M. L. Absorbed dose fraction for ^{87}Rb β particles. *Ancient TL* **20**, 25–28 (2002).
48. Richter, D., Richter, A. & Dornich, K. Lxsys — A new system for luminescence research. *Geochronometria* **40**, 220–228 (2013).
49. Buylaert, J. P. *et al.* A robust feldspar luminescence dating method for Middle and Late Pleistocene sediments. *Boreas* **44**, 407–411 (2012).
50. Duller, G. A. T. Assessing the error on equivalent dose estimates derived from single aliquot regenerative dose measurements. *Ancient TL* **25**, 15–24 (2007).
51. Duller, G. A. T. The Analyst software package for luminescence data: overview and recent improvement. *Ancient TL* **33**, 35–42 (2015).
52. Duller, G. A. T. *Analyst v4.31.7 User manual*. Technical report, 77 pages (2015).
53. Buylaert, J.-P. *et al.* Luminescence dating of the PASADO core 5022-1D from Laguna Potrok Aike (Argentina) using IRSL signals from feldspar. *Quatern. Sci. Rev.* **71**, 70–80 (2013).

54. Galbraith, R. F., Roberts, R. G., Laslett, G. M., Yoshida, H. & Olley, J. M. Optical dating of single and multiple grains of quartz from jinnium rock shelter, northern Australia: part i, experimental design and statistical models. *Archaeometry* **41**, 339–364 (1999).
55. Trautmann, T., Krbetschek, M. R., Dietrich, A. & Stolz, W. Feldspar radioluminescence: a new dating method and its physical background. *J. Lumin.* **85**, 45–58 (1999).
56. Frouin, M., Huot, S., Mercier, N., Lahaye, C. & Lamothe, M. The issue of laboratory bleaching in the infrared-radiofluorescence dating method. *Radiat. Meas.* **81**, 212–217 (2015).
57. Huot, S., Frouin, M. & Lamothe, M. Evidence of shallow TL peak contributions in infrared radiofluorescence. *Radiat. Meas.* **81**, 237–241 (2015).
58. Richter, D., Pintaske, R., Dornich, K. & Krbetschek, M. A novel beta source design for uniform irradiation in dosimetric applications. *Ancient TL* **30**, 57–63 (2012).
59. Kreutzer, S. *et al.* Always remain suspicious: a case study on tracking down a technical artefact while measuring IR-RF. *Ancient TL* **35**, 20–30 (2017).
60. Kreutzer, S. *et al.* Introducing an R package for luminescence dating analysis. *Ancient TL* **1**, 1–8 (2012).
61. Dietze, M. *et al.* The abanico plot: visualising chronometric data with individual standard errors. *Quatern. Geochronol* **31**, 12–18 (2016).
62. Dietze, M. & Kreutzer, S. plot_KDE(): Plot kernel density estimate with statistics. Function version 3.5.5. In: Kreutzer, S., Burow, C., Dietze, M., Fuchs, M. C., Schmidt, C., Fischer, M., Friedrich, J. *Luminescence: Comprehensive Luminescence Dating Data Analysis. R package version 0.8.4*, <https://CRAN.R-project.org/package=Luminescence> (2018).
63. Rees-Jones, J. Optical dating of young sediments using fine-grain quartz. *Ancient TL* **13**, 9–14 (1995).
64. Durcan, J. A., King, G. E. & Duller, G. A. T. DRAC: Dose Rate and Age Calculator for trapped charge dating. *Quatern. Geochron.* **28**, 54–61 (2015).

Acknowledgements

We thank His Royal Highness Prince Sultan bin Salman, President of the Saudi Commission for Tourism and National Heritage, and the Vice Presidents for Antiquities and Museums, for permission to carry out fieldwork in Saudi Arabia. EMLS and HSG would like to thank the British Academy for supporting this research. EMLS also thanks the Marie Skłodowska-Curie Actions (aWARE project grant 794117). J.-L.S and M.F. acknowledge generous support by the John Fell Fund (Oxford University) and the European Research Council (ERC grant 324139 awarded to Prof. T. Higham). A.M.A. would like to thank the Research center at the College of Tourism & Archaeology, King Saud University for their support. MDP acknowledges generous support from the European Research Council (Advanced Grant 295719 PALAEODESERTS: Climate Change and Hominin Evolution in the Arabian Desert: Life and Death at the crossroads of the Old World). We thank Ian R. Cartwright (Institute of Archaeology, University of Oxford) for the photograph in Figure 4c.

Author Contributions

All authors contributed towards the writing of the paper. The research was conceived by M.D.P., A.A. and C.S. Excavations at Saffaqah were conducted by C.S., H.S.G., P.C., L.C.-B., P.S.B., N.A.D., A.P., R.J. and A.A.-O. Artefact spatial data was processed and explored by J.B. and P.C. Chronometric dating was conducted by L.C.-B., M.F. and J.-L.S.

Additional Information

Supplementary information accompanies this paper at <https://doi.org/10.1038/s41598-018-35242-5>.

Competing Interests: The authors declare no competing interests.

Publisher's note: Springer Nature remains neutral with regard to jurisdictional claims in published maps and institutional affiliations.



Open Access This article is licensed under a Creative Commons Attribution 4.0 International License, which permits use, sharing, adaptation, distribution and reproduction in any medium or format, as long as you give appropriate credit to the original author(s) and the source, provide a link to the Creative Commons license, and indicate if changes were made. The images or other third party material in this article are included in the article's Creative Commons license, unless indicated otherwise in a credit line to the material. If material is not included in the article's Creative Commons license and your intended use is not permitted by statutory regulation or exceeds the permitted use, you will need to obtain permission directly from the copyright holder. To view a copy of this license, visit <http://creativecommons.org/licenses/by/4.0/>.

© The Author(s) 2018